Manganese-Enhanced MRI of Human Choroidal Melanoma Xenografts

Rod D. Braun[1,2], **Marius Gradianu**[1], **Kerry S. Vistisen**[1], **Robin L. Roberts**[1], and **Bruce A. Berkowitz**[1,3]

[1]Department of Anatomy and Cell Biology, Wayne State University School of Medicine, Wayne State University, Detroit, Michigan

[2]Barbara Ann Karmanos Cancer Institute, Wayne State University, Detroit, Michigan

[3]Kresge Eye Institute, Wayne State University, Detroit, Michigan

Abstract

Purpose—To test the hypothesis that the structure and function of an experimental human choroidal melanoma xenograft and neighboring non-tumor-bearing retina can be simultaneously assessed by using manganese-enhanced MRI (MEMRI).

Methods—Spheroids grown from the human choroidal melanoma cell line C918 were implanted in the superior suprachoroidal space of 11 *WAG/Nij-rnu* nude rats. Two weeks later, MRI data were collected 4 hours after intraperitoneal injection of saline or $MnCl_2$, an MRI contrast agent that can act as a biomarker of cellular demand for ions, such as calcium. The following parameters were measured: (1) tumor signal intensity, (2) inner and outer retinal signal intensity in non-tumor-bearing inferior retina, and (3) whole and inner retinal thickness of inferior retina. Separate MEMRI experiments were performed on spheroids in vitro after $MnCl_2$ exposure and washing.

Results—In vitro, spheroids exposed to $MnCl_2$ retained sufficient Mn^{2+} to demonstrate contrast enhancement during MEMRI. In vivo, injection of $MnCl_2$ resulted in a 30% increase in tumor signal intensity compared with tumors in rats injected with saline ($P < 0.05$). In inferior retina of tumor-bearing eyes, outer retinal signal intensity increased by 17% relative to a similar region in control eyes ($P < 0.05$), but there was no change in the inferior inner retinal intensity. Total retinal thickness of the inferior retina in the tumor-bearing eyes increased by 8%, compared with that in the non-tumor-bearing eyes ($P < 0.05$).

Conclusions—The present identification of regions of enhanced Mn^{2+} uptake in choroidal melanoma and a somewhat unexpected edema and increased outer retinal ion demand in neighboring non-tumor-bearing retina highlights MEMRI as a potentially powerful method for noninvasively monitoring tumor progression and treatment response and efficacy.

Uveal melanoma is the most common intraocular malignancy in adults, accounting for 70% of all primary eye cancers.[1] Although eye-sparing therapies such as radiation are equivalent to enucleation in terms of long-term survival,[2] these treatments do not always succeed in saving the patient's vision.[3] Three to 5 years after plaque radiotherapy or proton beam therapy, only approximately 60% of all patients maintain a visual acuity better than 20/200.[4–6] Complications after proton beam therapy include radiation retinopathy,[7] papillopathy,[7] and cataract.[8] Given the incidence of ocular complications during treatment

Corresponding author: Rod D. Braun, Anatomy and Cell Biology, Wayne State Univ School of Medicine, 540 E. Canfield Avenue, Detroit, MI 48201; rbraun@med.wayne.edu.

of choroidal melanoma, existing therapies must be optimized and new, more tumor-specific treatments should be developed. To achieve this goal, methods are needed for simultaneous determination of the effects of treatments on tumor growth and on the structure and function of the neighboring non-tumor-bearing retina.

Recent studies in the retina and brain have made use of Mn^{2+} as an ion surrogate and a strong MRI contrast agent for functional manganese-enhanced MRI (MEMRI).[9–11] In the retina experiments, $MnCl_2$ was administered under different lighting conditions while the animal was outside the magnet. The resultant accumulation of Mn^{2+} ions in nonvascular retina was detected noninvasively as an enhancement in T_1-weighted MRI images.[9] Similarly, in brain experiments, administration of $MnCl_2$ during a functional task resulted in the accumulation of Mn^{2+} ions in activated brain structures and enhanced T_1-weighted MRI images.[10,11] These results indicate that accumulation of Mn^{2+} and the resultant MRI intensity enhancement are function dependent. Free Mn^{2+} ion has not yet been used to image tumors, although there is evidence that some tumors preferentially accumulate Mn^{2+}.[12] Based on these findings, we decided to test whether high-resolution MEMRI could be used to enhance the imaging of experimental human choroidal melanomas in the eyes of nude, athymic rats. In addition, because MEMRI has recently been used to determine retinal thickness and functional changes in ion demand in the inner and outer layers of the rat retina,[9] we also tested the hypothesis that structural and functional (i.e., ion demand) parameters of neighboring retina can be simultaneously monitored.

Materials and Methods

Animals

The mutant rat strain *WAG/RijHs-rnu* was used in this study, because these rats are athymic and permit the xenotransplantation of human tumor tissue into the choroid.[13] The *WAG/RijHs-rnu* rats were bred and housed in the Department of Laboratory Animal Resources (DLAR) facility at Wayne State University. All procedures were in accordance with the ARVO Statement for the Use of Animals in Ophthalmic and Vision Research and were approved by the Wayne State University Animal Investigation Committee.

Human Choroidal Melanoma Cell Line

The human choroidal melanoma cell line C918 was used in this study. This cell line was derived from a patient's tumor at the University of Iowa in the 1990s.[14] The cells were maintained in RPMI medium+10% fetal bovine serum (FBS)+antibiotic. We have demonstrated the reliable ability of these cells to generate tumor xenografts in the choroid of *WAG/RijHs-rnu* nude, athymic rats.[13]

Growth of Tumor Spheroids

C918 tumor spheroids (three-dimensional aggregations of tumor cells) were grown by using a modified version of the method described by Yuhas et al.[15] Agar (1%) was prepared in RPMI medium by sterilization for 30 minutes. While still hot, 20 mL of 1% agar was poured into the bottom of sterile 100×20-mm plastic Petri dishes. To initiate spheroid growth, 3×10^6 cells in 20 mL of RPMI+FBS+antibiotic were placed in each agar-coated Petri dish. The dishes were then placed in the incubator. Spheroids were implanted into the choroid when they were 200 to 500 μm in diameter and were used in the Mn^{2+} uptake study when they had been growing for 10 or 13 days.

Growth of Orthotopic Human Choroidal Melanoma Xenografts

C918 spheroids were implanted into the suprachoroidal space of rats as detailed previously.[13] Tumor implantation was performed under sterile conditions in a BSL2 safety

hood in the Wayne State DLAR facility. Rats were anesthetized with a ketamine-xylazine mixture (70/8 mg/kg IP) and proparacaine HCl (0.5%) was applied topically to the right eye as local anesthesia. The rat was placed under an operating microscope, and approximately five tumor spheroids in 1 μL of medium were injected into the suprachoroidal space with a 5-μL glass syringe (Model 65RNR; Hamilton Co., Reno, NV) equipped with a three-quarter-inch-long beveled 32-gauge needle (cat. no. 0160832, point style 4; Hamilton Co.). Antibiotic ointment was applied to the eye, and the rat was allowed to recover on the heating blanket before being returned to its cage. C918 spheroids were implanted in the right eyes of 11 rats.

MEMRI of Rat Eyes

After 14 days of tumor growth, awake rats were injected intraperitoneally on the right side with either 44 mg/kg MnCl$_2$ (0.1 M solution; $n = 6$) or an equivalent volume of saline ($n = 5$) and kept in the light.[9] After another 3.5 hours, rats were anesthetized with urethane (36% solution, intraperitoneally, 0.083 mL/20 g animal weight, prepared fresh daily; Aldrich, Milwaukee, WI). To maintain the core temperature, a recirculating heated water blanket was used. Rectal temperatures were continuously monitored throughout each experiment, as previously described.[16] MRI data were acquired on a 4.7-T system (Avance; Bruker, Karlsruhe, Germany) using a two-turn transmit-receive surface coil (1.0-cm diameter) placed over the eye. In all rats, left and right eyes were studied sequentially. Images were acquired using an adiabatic spin-echo imaging sequence (repetition time [TR] 350 seconds, echo time [TE] 16.7 ms, number of acquisitions [NA] 16, matrix size 256 × 512, slice thickness 600 μm, field of view 12 × 12 mm^2, 23 minutes/image).[17] A single transverse slice through the center of each eye (based on sagittal localizer images collected using the same adiabatic pulse sequence) was obtained for each rat.

Determination of Tumor Signal Intensity

Average signal intensities within the tumor were measured from the high-resolution MRI data of the tumor-bearing right eyes for all 11 rats, whether they received MnCl$_2$ or saline. The tumor area was selected and measured, and signal intensity was analyzed (Image; a freeware program available by ftp at zippy.nimh.nih.gov/ or at http://rsb.info.nih.gov/nih-image; developed by Wayne Rasband, National Institutes of Health, Bethesda, MD) and derived macros.[18] We controlled for changes in receiver gain differences between animals by setting the signal intensity of a fixed region of noise in each rat to a fixed value. Intensities were expressed as arbitrary units (AU).

Determination of Intraretinal Signal Intensity

Intraretinal signal intensities were measured from the high-resolution images of both eyes in the manganese-injected rats and the tumor-bearing eyes of the saline-injected rats.[9] For visualization and analysis purposes, in-house-written software was used to map the in situ image into a linear representation of each retina. Within each group, linearized retinas were either analyzed separately or averaged into a composite image. The inner and outer inferior retinal signal intensity data from 0.4 to 1 mm from the optic nerve were extracted from the inferior control or non-tumor-bearing retina for further analysis.

Determination of Retinal Thickness

From the MEMRI data, inner or total retinal thicknesses were measured as the radial distance between the anterior and middle edge (defined by its change in signal intensity) or posterior edges of the retina.[9] Six measurements at distances between 0.4 and 1 mm from the optic nerve were measured in the inferior retina of each image. Inner retinal thickness could not be determined in one set of eyes, because the rat may have been dark-adapted and

the inner– outer retina border was not distinguishable. Mean inferior values generated for each rat were used for paired comparisons.

For the saline-injected rats (i.e., without $MnCl_2$ injection), total retinal thicknesses in the inferior retina were measured as described earlier. Inner retinal thicknesses could not be measured, since the inner-outer retina is not readily distinguishable without Mn^{2+}.[9]

MEMRI of C918 Tumor Spheroids

After C918 spheroids had been grown for 10 or 13 days, they were washed, resuspended in RPMI medium, and divided into microcentrifuge tubes. Spheroids were then exposed to 0, 25, or 100 μM $MnCl_2$ in RPMI medium+10% FBS for 1 hour at 37°C. These $MnCl_2$ concentrations were chosen based on earlier in vitro studies investigating Mn^{2+} uptake by lymphocytes[19] and pancreatic islets.[20] The spheroids were resuspended every 10 minutes by agitation of the tubes. After the 1-hour exposure, the spheroids were washed, resuspended in RPMI+10% FBS, and put on ice. The microcentrifuge tubes were placed in the magnet, and MRI data were obtained. This experiment was performed in triplicate.

Statistical Analysis

Since the groups were relatively small and a normal distribution could not always be assumed, average tumor and retinal signal intensities were compared using the Mann-Whitney test. Similarly, the average retinal thickness and retinal intensity data of the control and tumor-bearing eyes were compared using the nonparametric Wilcoxon signed rank test. In all tests, $P < 0.05$ was considered statistically significant.

Results

MEMRI of C918 Human Choroidal Melanoma Spheroids

After exposure to 100 μM $MnCl_2$, spheroid signal intensity increased by 30% $\pm$ 22% (mean $\pm$ SD, $n = 3$), which is indicative of intracellular retention of Mn^{2+} (Fig. 1).

High-Resolution MRI of C918 Human Choroidal Melanoma Xenografts without $MnCl_2$ Injection

High-resolution, T_1-weighted images of the right eye revealed the presence of a C918 xenograft in the superior portion of the eye (Fig. 2A). Tumors were identified in all five rats injected with saline and appeared hyperintense relative to the retina and vitreous. In-plane tumor areas ranged from 1.5 to 3.2 mm^2, with an average area of 2.25 $\pm$ 0.76 mm^2 (mean $\pm$ SD, $n = 5$; Table 1).

High-Resolution MEMRI of C918 Human Choroidal Melanoma Xenografts with $MnCl_2$ Injection

Signal enhancements consistent with retention of Mn^{2+} were evident within all six tumors in rats injected with $MnCl_2$ (Fig. 2B). In-plane tumor area ranged from 1.5 to 6.4 mm^2, with an average area of 3.89 $\pm$ 2.33 mm^2 (mean $\pm$ SD, $n = 6$, Table 1). There was no difference between the areas of the tumors injected with saline and those injected with $MnCl_2$ (Table 1, $P = 0.537$). In the $MnCl_2$-injected rats, the average intensity of the tumors was 30% greater than the corresponding value in the saline-injected rats (Table 1, $P = 0.030$).

MEMRI of Retina in Tumor-Bearing Rats

In the rats injected with $MnCl_2$, signal enhancements were evident throughout the retina in both the tumor-bearing right eye (Fig. 2) and the control left eye. In the tumor-bearing right eye, the signal intensities of the inferior inner retina (178.5 $\pm$ 7.3 AU, $n = 6$) and outer retina

$(182.7 \pm 9.3$ AU, $n = 6)$ were significantly greater after injection of $MnCl_2$ than the corresponding values in the inferior retina after injection of saline (inner retina: 76.4 ± 11.0 AU, outer retina: 74.8 ± 7.2 AU, $n = 5$, $P = 0.004$).

As expected for light-adapted control retinas after injection of $MnCl_2$, the average signal intensity of the inner layer of the inferior retina of the control eyes was significantly greater than the intensity of the outer retina (Fig. 3A, Table 2).[9] In contrast, in the tumor-bearing eyes, inner and outer retina signal intensities were similar (Fig. 3B, Table 2).

Visual comparison of the linearized spatial maps of average signal intensity of the inferior retina in each group revealed differences in the Mn^{2+} enhancement patterns (Fig. 3). The intensity of the non-tumor-bearing inferior outer retina in the tumor-bearing eyes was $16.5 \pm 7.6\%$ (mean $\pm$ SD, $n = 6$, $P = 0.031$) higher than that of the outer retina in the corresponding control eyes (Fig. 3, Table 2). In contrast, no difference was found in the average intensities of the non-tumor-bearing inferior inner retinas of the tumor-bearing eyes compared with the control eyes (Table 2; $P = 0.563$). Similarly, in the absence of Mn^{2+}, the signal intensity of the inferior inner retina (76.4 ± 11.0 AU, $n = 5$) was not significantly different from that of the outer retina (74.8 ± 7.2 AU, $n = 5$, $P = 0.813$) in the tumor-bearing eyes.

Retinal Thickness

The total retinal thickness of the inferior retina in the tumor-bearing eye was $7.7\% \pm 95\%$ greater than that of the corresponding control eye (Table 2, $P = 0.031$). There was no difference between the thickness of the inferior inner retina of the tumor-bearing eye and that of the corresponding control eye (Table 2). The total thickness of the inferior retina in the tumor-bearing eye of the saline-injected rats ($253.3 \pm 4.8 \mu m$; $n = 5$), was not significantly different from the thickness of the inferior retina in the $MnCl_2$-injected rats ($246.1 \pm 21.8 \mu m$; $n = 6$, $P = 0.082$).

Discussion

This study has resulted in two significant new findings. First, tumor cells were shown to retain a significant amount of Mn^{2+} after exposure in vitro and in vivo, resulting in MRI signal enhancement. Second, it was demonstrated that the structure and function of neighboring non-tumor-bearing retina was affected by the presence of the melanoma. These data lay the foundation for future studies of treatment efficacy for choroidal melanoma.

High-Resolution MEMRI of C918 Human Choroidal Melanoma Xenografts

As expected, high-resolution MRI imaging of the rat eye, even without infusion of $MnCl_2$, permitted the visualization of human choroidal melanoma xenografts growing in the suprachoroidal space in this nude rat model. As is the case with most choroidal melanomas in humans,[21] the orthotopic xenografts were hyperintense compared with the intensity of the vitreous (Fig. 2). Injection of $MnCl_2$ greatly enhanced the tumor-retina contrast.

The present finding of substantial intraocular tumor uptake of Mn^{2+} is consistent with the results of a previous nonocular study, in which the uptake of radioactively labeled Mn^{2+} was five times higher in a brain tumor than in the normal surrounding brain.[12] However, that study did not determine whether the free Mn^{2+} ion was within the tumor cells or was extracellular. To investigate, we examined Mn^{2+} uptake by tumor spheroids in vitro. The C918 cells clearly internalized the Mn^{2+}, since, even after thorough rinsing, exposure of the spheroids to $MnCl_2$ resulted in contrast enhancement (Fig. 1).

Although Mn^{2+} accumulation has been related to increased neuronal activity[9–11] and increased pancreatic islet function,[20] the exact mechanism behind the increased uptake in

tumors is not known. Because Mn^{2+} can enter cells through voltage-gated and voltage-independent calcium channels,[22,23] it may serve as a surrogate marker of Ca^{2+} uptake. Since Ca^{2+} uptake is associated with increased proliferation,[24,25] the increased Mn^{2+} accumulation may mimic increased Ca^{2+} uptake by mitotically active tumor cells. Alternatively, because Ca^{2+} also plays a role in angiogenesis,[26] the increased Mn^{2+} uptake could be a marker of sites of tumor-induced angiogenic activity. Future studies are needed to elucidate the mechanism of Mn^{2+} accumulation in the tumor cells.

Effects of the Presence of the Tumor on Neighboring Retina

One of the major advantages of using MEMRI in this xenograft model is the ability to obtain simultaneous structural and functional information on the tumor and on the neighboring retina in the inferior non–tumor-bearing portion of the eye. In the control left eye, the inferior inner retinal intensity was greater than that in the inferior outer retina (Fig. 3; Table 2), which agrees with earlier results in the normal light-adapted rat retina.[9] In contrast, in the tumor-bearing eye, we found high Mn^{2+} uptake in both the inferior inner and outer layers of the retina, which is the pattern typically found in dark-adapted conditions,[9] even though these animals were light adapted. In particular, signal intensity or Mn^{2+} accumulation increased in the inferior outer retina of the tumor-bearing eyes compared with the control eyes (Table 2). The mechanism behind this increase in outer retinal Mn^{2+} uptake is not known. It may be caused by a tumor-induced change in intraocular pressure that could alter retinal function. Alternatively, it could be attributable to the direct effect of molecules released by the tumor on the retinal tissue. Regardless of the mechanism behind the Mn^{2+} accumulation, the function of the inferior outer retina, as assessed by ion demand, was adversely affected by the presence of the tumor, even though this section of retina was not directly involved in the tumor growth.

It was also demonstrated that the presence of the tumor in the superior retina caused an increase in the total thickness of the inferior retina, suggestive of edema (Table 2). The mechanism behind this edema is unclear, but it may be related to a secondary effect of the tumor on ocular function or the direct effect of secretory products on the retina.

The ability to monitor retinal function and thickness simultaneously in the tumor-bearing eye is an important advantage of MEMRI imaging in this model. We anticipate that MEMRI will allow the determination of bystander effects of tumor growth on the neighboring retina. Perhaps more important, with this technique, the impact of various treatments on the tumor and on the neighboring retina can be evaluated. Minimizing collateral damage to the retina is a serious issue in current treatments and in the development of new treatment modalities for choroidal melanoma.[4–6]

Summary

For the first time, systemic injection of a $MnCl_2$ solution has been used to image a tumor by using MEMRI. The imaging of a human choroidal melanoma xenograft transplanted into the eye of a nude rat permitted the simultaneous evaluation of the tumor and the neighboring retina in the same eye. Mn^{2+} was taken up by the tumor, which resulted in contrast enhancement during MEMRI imaging. The retina in the inferior portion of the eye, which was not in direct contact with the tumor, was adversely affected by the presence of the melanoma. Inferior outer retinal MEMRI intensity was altered in those eyes, and the inferior retina was edematous. The use of the MEMRI technique in this choroidal melanoma model will permit the study of the impact of tumor growth on the neighboring retina and will allow the simultaneous evaluation of treatment-related side effects in the same eye.

The practical applicability of this method in humans has not yet been evaluated. However, we note that a manganese-based contrast agent (Mangafodipir Trisodium [Teslascan]; GE Healthcare, Princeton, NJ) already has FDA approval and that motion–artifact free high-resolution MRIs of the human retina can be routinely collected.[27–30] These considerations raise the possibility of clinically monitoring choroidal melanoma progression and/or treatment response using MEMRI in patients.

Acknowledgments

References

1. Sahel JA, Albert DM. Intraocular melanomas. Cancer Treat Res. 1993; 65:161–199. [PubMed: 8104021]

2. Diener-West M, Earle JD, Fine SL, et al. The COMS randomized trial of iodine 125 brachytherapy for choroidal melanoma, III: initial mortality findings. COMS Report No. 18. Arch Ophthalmol. 2001; 119:969–982. [PubMed: 11448319]

3. Finger PT. Radiation therapy for choroidal melanoma. Surv Ophthalmol. 1997; 42:215–232. [PubMed: 9406368]

4. COMS. Collaborative ocular melanoma study (COMS) randomized trial of I-125 brachytherapy for medium choroidal melanoma: I. visual acuity after 3 years COMS report no. 16. Ophthalmology. 2001; 108:348–366. [PubMed: 11158813]

5. Shields CL, Shields JA, Cater J, et al. Plaque radiotherapy for uveal melanoma: long-term visual outcome in 1106 consecutive patients. Arch Ophthalmol. 2000; 118:1219–1228. [PubMed: 10980767]

6. Gragoudas ES, Lane AM, Regan S, et al. A randomized controlled trial of varying radiation doses in the treatment of choroidal melanoma. Arch Ophthalmol. 2000; 118:773–778. [PubMed: 10865313]

7. Gragoudas ES, Li W, Lane AM, Munzenrider J, Egan KM. Risk factors for radiation maculopathy and papillopathy after intraocular irradiation. Ophthalmology. 1999; 106:1571–1578. [PubMed: 10442906]

8. Gragoudas ES, Egan KM, Walsh SM, Regan S, Munzenrider JE, Taratuta V. Lens changes after proton beam irradiation for uveal melanoma. Am J Ophthalmol. 1995; 119:157–164. [PubMed: 7832221]

9. Berkowitz BA, Roberts R, Goebel DJ, Luan H. Noninvasive and simultaneous imaging of layer-specific retinal functional adaptation by manganese-enhanced MRI. Invest Ophthalmol Vis Sci. 2006; 47:2668–2674. [PubMed: 16723485]

10. Lin YJ, Koretsky AP. Manganese ion enhances T_1-weighted MRI during brain activation: an approach to direct imaging of brain function. Magn Reson Med. 1997; 38:378–388. [PubMed: 9339438]

11. Yu X, Wadghiri YZ, Sanes DH, Turnbull DH. In vivo auditory brain mapping in mice with Mn-enhanced MRI. Nat Neurosci. 2005; 8:961–968. [PubMed: 15924136]

12. Tamano H, Enomoto S, Oku N, Takeda A. Preferential uptake of zinc, manganese, and rubidium in rat brain tumor. Nucl Med Biol. 2002; 29:505–508. [PubMed: 12031887]

13. Braun RD, Abbas A. Orthotopic human choroidal melanoma xenografts in nude rats with aggressive and nonaggressive PAS staining patterns. Invest Ophthalmol Vis Sci. 2006; 47:7–16. [PubMed: 16384938]

14. Daniels KJ, Boldt HC, Martin JA, Gardner LM, Meyer M, Folberg R. Expression of type VI collagen in uveal melanoma: its role in pattern formation and tumor progression. Lab Invest. 1996; 75:55–66. [PubMed: 8683940]

15. Yuhas JM, Li AP, Martinez AO, Ladman AJ. A simplified method for production and growth of multicellular tumor spheroids. Cancer Res. 1977; 37:3639–3643. [PubMed: 908012]

16. Berkowitz BA, Ito Y, Kern TS, McDonald C, Hawkins R. Correction of early subnormal superior hemiretinal ΔPO_2 predicts therapeutic efficacy in experimental diabetic retinopathy. Invest Ophthalmol Vis Sci. 2001; 42:2964–2969. [PubMed: 11687543]

17. Schupp DG, Merkle H, Ellermann JM, Ke Y, Garwood M. Localized detection of glioma glycolysis using edited 1H MRS. Magn Reson Med. 1993; 30:18–27. [PubMed: 8371670]

18. Berkowitz BA, Kowluru RA, Frank RN, Kern TS, Hohman TC, Prakash M. Subnormal retinal oxygenation response precedes diabetic-like retinopathy. Invest Ophthalmol Vis Sci. 1999; 40:2100–2105. [PubMed: 10440266]

19. Aoki I, Takahashi Y, Chuang KH, et al. Cell labeling for magnetic resonance imaging with the T_1 agent manganese chloride. NMR Biomed. 2006; 19:50–59. [PubMed: 16411253]

20. Gimi B, Leoni L, Oberholzer J, et al. Functional MR microimaging of pancreatic beta-cell activation. Cell Transplant. 2006; 15:195–203. [PubMed: 16719054]

21. Peyster RG, Augsburger JJ, Shields JA, Hershey BL, Eagle R Jr, Haskin ME. Intraocular tumors: evaluation with MR imaging. Radiology. 1988; 168:773–779. [PubMed: 3406407]

22. Dryselius S, Grapengiesser E, Hellman B, Gylfe E. Voltage-dependent entry and generation of slow Ca^{2+} oscillations in glucose-stimulated pancreatic beta-cells. Am J Physiol. 1999; 276:E512–518. [PubMed: 10070018]

23. Crossgrove JS, Yokel RA. Manganese distribution across the blood-brain barrier. IV. Evidence for brain influx through store-operated calcium channels. Neurotoxicology. 2005; 26:297–307. [PubMed: 15935202]

24. Lipskaia L, Lompre AM. Alteration in temporal kinetics of Ca^{2+} signaling and control of growth and proliferation. Biol Cell. 2004; 96:55–68. [PubMed: 15093128]

25. Munaron L, Antoniotti S, Lovisolo D. Intracellular calcium signals and control of cell proliferation: how many mechanisms? J Cell Mol Med. 2004; 8:161–168. [PubMed: 15256064]

26. Kohn EC, Alessandro R, Spoonster J, Wersto RP, Liotta LA. Angiogenesis: role of calcium-mediated signal transduction. Proc Natl Acad Sci USA. 1995; 92:1307–1311. [PubMed: 7533291]

27. Adam G, Brab M, Bohndorf K, Gunther RW. Gadolinium-DTPA-enhanced MRI of intraocular tumors. Magn Reson Imaging. 1990; 8:683–689. [PubMed: 2266793]

28. Berkowitz BA, McDonald C, Ito Y, Tofts PS, Latif Z, Gross J. Measuring the human retinal oxygenation response to a hyperoxic challenge using MRI: eliminating blinking artifacts and demonstrating proof of concept. Magn Reson Med. 2001; 46:412–416. [PubMed: 11477648]

29. Trick GL, Edwards P, Desai U, Berkowitz BA. Early supernormal retinal oxygenation response in patients with diabetes. Invest Ophthalmol Vis Sci. 2006; 47:1612–1619. [PubMed: 16565400]

30. Trick GL, Liggett J, Levy J, et al. Dynamic contrast enhanced MRI in patients with diabetic macular edema: initial results. Exp Eye Res. 2005; 81:97–102. [PubMed: 15978260]
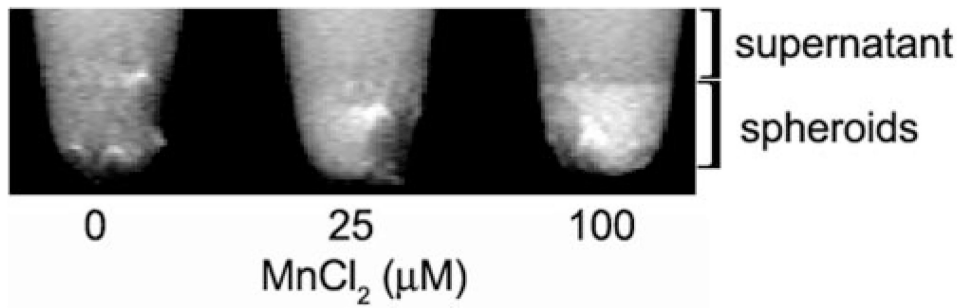
Figure 1.
Representative high-resolution MRIs ($46.8 \times 23.4 \times 600 \ \mu m^3$) of C918 spheroids 4 hours after exposure to $MnCl_2$ for 1 hour at 37°C. The spheroids were pooled at the bottom of the tube.
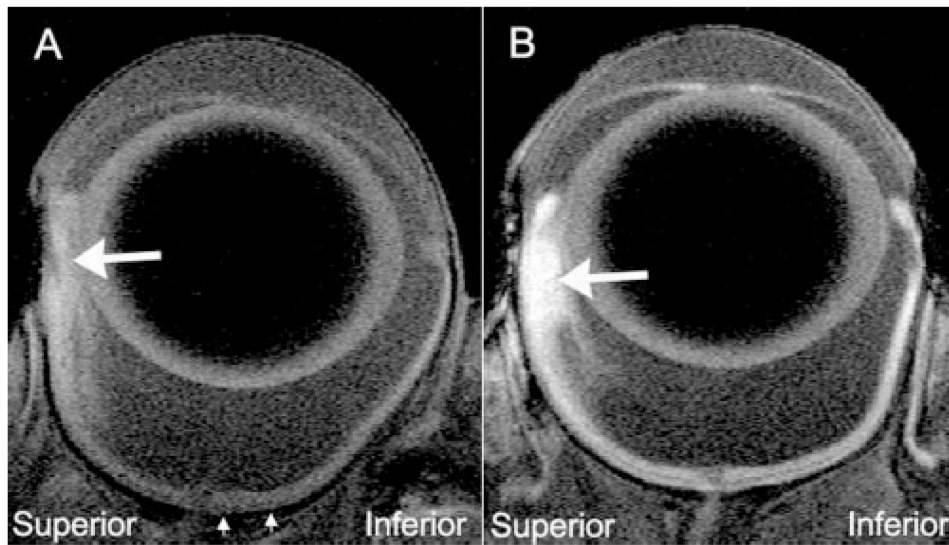
Figure 2.
Representative high-resolution MRIs of tumor-bearing eyes 4 hours after IP saline injection (**A**) or $MnCl_2$ injection (**B**). Comparison of peripheral superior and inferior retina clearly identifies the tumors (*large arrows*). The tumor areas were (**A**) 1.54 and (**B**)1.87 mm^2. The average intensities of these tumors were (**A**) 122.1 AU and (**B**) 167.5 AU. Note that the data in Figure 3 was derived from the region of inferior retina located between the *small arrows*.
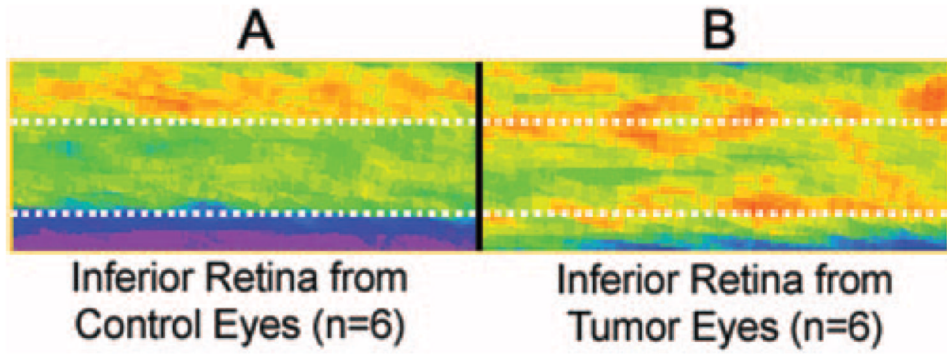
Figure 3.
Pseudocolor images of average retinal signal intensity in the inferior retina (see Fig. 2) of the control left eye (**A**) and the inferior retina of the tumor-bearing right eye (**B**). The same pseudocolor scale was used for both images, where *blue* to *green* to *yellow* to *red* represent lowest to highest signal intensity. *Top dotted line*: presumed boundary between the inner and outer retina of the control eye; *bottom dotted line*: boundary of the posterior aspect of the control eye.

Table 1

Average Signal Intensity of Tumor after Saline or $MnCl_2$ Injection

Injection	In-Plane Tumor Area (mm^2)	Average Signal Intensity (AU)	Number of Rats
Saline	2.25 ± 0.76	114.1 ± 131	5
$MnCl_2$	3.89 ± 2.33	148.9 ± 25.5	6
P^*	0.537	0.030	

Data are expressed as the mean ± SD.

*
Saline- versus MnCl2-injected rats; Mann-Whitney rank sum test.

Table 2

Average Retinal Thickness and Average Signal Intensity of the Inferior Retina in the Control Left Eye and the Tumor-Bearing Right Eye after MnCl₂ Injection

Eye	Total Inferior Retinal Thickness (μm)	Inner Inferior Retinal Thickness (μm)	Inner Retinal Intensity (AU)	Outer Retinal Intensity (AU)	Rats (n)	P Inner vs. Outer Intensity
Control	228.6 ± 6.9	107.7 ± 3.2	181.0 ± 11.5	157.5 ± 15.4	6	0.031
Tumor-bearing	246.1 ± 21.8	118.6 ± 154	178.5 ± 7.3	182.7 ± 9.3	6	0.438
Rats (n)	6	5	6	6		
P*	0.031	0.188	0.563	0.031		

Data are expressed as the mean ± SD.

*
Control versus tumor-bearing eyes or inner and outer retina; Wilcoxon signed rank test.